Journal of Molecular Liquids 222 (2016) 1041–1050

Contents lists available at ScienceDirect

Journal of Molecular Liquids

journal homepage: www.elsevier.com/locate/molliq

Biogenic silver nanoparticles – Synthesis, characterization and its potential against cancer inducing bacteria

M. Jannathul Firdhouse, P. Lalitha *

Department of Chemistry, Avinashilingam Institute for Home Science and Higher Education for Women, Coimbatore -641043, Tamil Nadu, India

ARTICLE INFO

Article history:
Received 14 February 2016
Received in revised form 22 July 2016
Accepted 31 July 2016
Available online 5 August 2016

Keywords:
Silver nanoparticles
E.coli
Antibacterial activity
TEM

ABSTRACT

Biogenic synthesis of silver nanoparticles was achieved using extracts from sixteen commonly available plants by sonication method. The formation of AgNPs was confirmed by UV–Visible spectral, XRD and TEM analyses. The results of TEM analysis reveal mostly spherical-shaped AgNPs of size 5–25 nm AgNPs. Antibacterial assay carried out for the biosynthesized AgNPs against bacteria (*Escherichia coli, Salmonella paratyphi, Staphylococcus aureus* and *Bacillus subtilis*) disclosed excellent antibacterial activity. This may be due to the small-sized nature of particles diffusing through the agar resulting in good antimicrobial activity.

1. Introduction

Nanotechnology deals with the development of experimental processes for the synthesis of nanoparticles of different sizes, shape and controlled dispersity. Nanoscale materials usually range from 1 to 100 nm and are an emerging area of nanoscience and nanotechnology [1]. Nanoparticles find applications in optoelectronic devices [2], environment friendly energy systems, biosensors [3], biomedical imaging [4], medical textiles [5] and drug delivery purposes [6]. An enormous number of publications and patents, evidence the exploitation of nanotechnology [7].

Nanomedicine is an upcoming field that could potentially make a major impact on human health [8]. It has also gained emergent interest due to its superior properties with functional versatility and serves as a potential tool for treating various diseases [9–11]. Metal nanoparticles possess unique properties, much different from that of bulk materials. Nanoparticle based cellular delivery has been extensively used owing to their properties like accessibility, high functionality and competence in targeting specific areas for the release of drugs [12–15].

Infections caused by bacteria are prone to cause acute diseases, but in the present scenario, bacteria are also responsible for chronic infections, diseases and cancers [16]. Studies involving the characterization of bacteria present within the tumour tissues are reported [17]. *Helicobacter pylori* is reported to cause both gastric cancer and mucosa associated lymphoid tissue (MALT) lymphoma [18]. *Streptococcus bovis* (colon cancer) [19] and *Chlamydia pneumonia* play a part in lung cancer [20].

Researchers have postulated some hypothetical mechanisms for bacteria-induced carcinogenesis *via* chronic inflammation due to constant bacterial infections, secondary metabolites and toxins produced by bacterial infections. In general, these infections cause cancer in direct proportion to their chronicity, the longer the inflammatory process persists and the more likely malignancy is to develop.

World Health Organization (WHO) declared antibiotic - resistance a "major global threat" to the public because of high levels of the resistant *Escherichia coli* towards cephalosporin and fluoroquinolones in Southeast Asia region (**Times of India, April 2014**). *Escherichia coli* produce toxins which cause secretory diarrhoea. Ulcerative colitis and Crohn's disease are inflammatory bowel diseases with potency of developing into colorectal cancer. The enteropathogenic bacteria *E. coli* causes effacing lesions in the large intestine, expressed hemagglutinins in 39% of Crohn's cases and 38% of cancers [21]. In some regions, one-fourth of infections are due to methicillin resistant *Staphylococcus aureus* (MRSA) which cause 64% death compared to the non-resistant infections. *Salmonella typhi* causes typhoid, which lead to chronic bacterial carriage in the gall bladder. The carriers of *S. paratyphi* have 8.47 times possibility of developing gall bladder cancer contrast to acute typhoid patients [22,23]. An investigation on patients with severe *Salmonella* infections disclosed lack of Interleukin-12 (IL-12Rβ1) expression which leads to immune deficiency [24].

Staphylococcus aureus is the main cause of respiratory tract, surgical site and cardiovascular infections and also cause pneumonia, nosocomial bacteremia *etc.* This bacterium is difficult to treat due to its resistance towards antimicrobial drugs. In 2010–2011, outbreaks of staphylococcal food poisoning were reported in Australia and New Zealand. Fatal rate was reported as 4.4% for the elderly people and 0.03% for general public [25,26].

* Corresponding author.
E-mail address: goldenlalitha@gmail.com (P. Lalitha).

http://dx.doi.org/10.1016/j.molliq.2016.07.141
0167-7322/

In our present work, spherical-shaped silver nanoparticles of size <50 nm have been prepared using 16 different plant extracts under sonication method. To overcome the aforesaid clinical problems associated in cancer, we have particularly chosen *E. coli, S. typhi, B. subtilis* and *S. aureus* for the antibacterial study with plant-mediated silver nanoparticles by well diffusion method. All the synthesized silver nanoparticles showed good zone of inhibition compared to that of the standard Gentamicin.

2. Materials and methods

2.1. Materials

The fresh parts of the selected plants (*Amaranthus dubius* (AK), *Amaranthus polygonoides* (SK), *Alternanthera sessilis* (PGK), *Portulaca oleracea* (PAK), *Pisonia grandis* (PG), *Eichhornia crassipes* (WH), *Rosmarinus officinalis* (RM) and powdered form of *Tabebuia heterophylla* (TH), *Kedrostis foetidissima* (KFL), *Curcumba rubescens* (CR), *Alpinia calcarata* (APC), *Ocimum basilicum* (OB), *Annona reticulata* (ARL), *Sterculia foetida* (SF), *Acorus calamus* (AC) and *Rhaphidophora aurea* (MP) were collected from in and around Coimbatore district (Table 1).

2.2. Preparation of aqueous extracts

Each plant (20 g) was weighed, washed thoroughly thrice with distilled water and cut into fine pieces. Each plant material was boiled for 5 min with 100 ml millipore water in a 500 ml Erlenmeyer flask. The prepared solutions were filtered using Whatmann filter paper No. 42 to remove the plant debris, sonicated for 15 min and refrigerated at −4 °C for further studies. The filtrate (designated as aqueous extract) was used within a week to avoid the annihilation of phytoconstituents.

2.3. Synthesis of silver nanoparticles

The varied concentrations of silver nitrate (designated as *C*1, C2, C3, *C*4 and C5) with constant volume of each plant extract constitute one set. The ratio of aqueous extracts of plants and silver nitrate as given below was fixed based on preliminary experiments.

(i) The prepared aqueous extracts of the plants (AK, SK, PGK, PAK, MP and RM) and silver nitrate (3 mM) solution were mixed in five different ratios as 1:6, 1:7, 1:8, 1:9 and 1:10 are sonicated using an ultrasonic bath (Ultrasonic's (1.5 l (H)).
(ii) The concentration of silver nitrate was varied (1, 2, 3, 4 and 5 ml) and added to a constant volume (1 ml) of (SF, ARL, AC, CR, OB and APC) extracts and sonicated.
(iii) Different concentrations of 3 mM silver nitrate (6, 7, 8, 9 and 10 ml) were treated with 5 ml aqueous extracts of (TH, WH, PG and KFL) and sonicated.

Table 1
Botanical names of the selected plants.

S. No	Plants chosen for the study	Acronyms	Parts used
1.	*Amaranthus dubius*	AK	Whole
2.	*Amaranthus polygonoides*	SK	Whole
3.	*Alternanthera sessilis*	PGK	Whole
4.	*Portulaca oleracea*	PAK	Whole
5.	*Eichhornia crassipes*	WH	Whole
6.	*Kedrostis foetidissima*	KFL	Leaves
7.	*Curcuma rubescens*	CR	Root
8.	*Rosemarnius officinalis*	RM	Whole
9.	*Tabebuia heterophylla*	TH	Flowers
10	*Ocimum basilicum*	OB	Leaves
11.	*Alpinia calcarata*	APC	Root
12.	*Sterculia foetida*	SF	Root
13.	*Acorus calamus*	AC	Stem
14.	*Annona reticulata*	ARL	Leaves
15.	*Rhaphidophora aurea*	MP	Aerial roots
16.	*Pisonia grandis*	PG	Leaves

The aforesaid mixtures of the sixteen plant extract with silver nitrate were sonicated until reddish brown colour appeared. The formation of silver nanoparticles were monitored by UV–visible spectroscopy. The products were collected following centrifugation at 5000 rpm for 5 min and were sonicated with ethanol and then dried for 24 h at room temperature.

2.4. Characterization of synthesized silver nanoparticles

The synthesized silver nanoparticles were analyzed by UV–Visible spectroscopy using a Double beam spectrophotometer 2202-(Systronics). The scanning range of the samples was 300–500 nm at a scan speed of 150 nm/min. XRD analysis was carried out for the nanosilver coated on a glass substrate using X'pert Pro X-ray diffractometer with a Cu Kα radiation ($\lambda = 1.54060$ Å) monochromatic filter operated at 45 kV and 30 mA over the range of $2\theta = 10–80°$ with scanning rate 2° / min. The nanodimension of the synthesized AgNPs was established through recording TEM images using FEI's Tecnai G2 Transmission Electron Microscope. The imaging of the sonicated AgNPs was enabled by depositing a few drops of suspension on a carbon film 200 mesh, copper grid of 2.8 mm diameter and the solvent was dried in a desiccator at room temperature prior to recording TEM.

2.5. Antibacterial study of the biosynthesized AgNPs

2.5.1. Microorganisms used for the study

Antibacterial activity was carried out for the biosynthesized AgNPs by Agar-well diffusion method against cancer inducing gram negative (*Escherichia coli* and *Salmonella paratyphi*) and nosocomial infection gram positive (*Staphylococcus aureus* and *Bacillus subtilis*) bacteria.

2.5.2. Antibacterial screening of biosynthesized AgNPs

Four bacterial strains (*E. coli, S. paratyphi, B. subtilis* and *S. aureus*) were inoculated into the nutrient broth under aseptic conditions and incubated at 37 °C for 18 h. After the incubation period, the bacteria to be tested were swabbed on the nutrient agar plate using sterile cotton swab. Each bacterium was swabbed separately and each plate was divided into six parts. Wells (6 mm) were made on a Muller Hinton Agar plate using a sterile cork borer under aseptic conditions. Calculated volumes of different plant-mediated silver nanoparticles (AKG, SKG, PGKG, PAKG, PGG, KFLG, WHG, THG, OBG, APCG, CRG, RMG, MPG, ARLG, ACG and SFG) (20 μl containing 600 μg) Gentamicin (control) were loaded onto the marked wells with the help of micropipette under aseptic conditions and plates were incubated at 37 °C for 24 h. Each experiment was carried out in triplicate under identical conditions to ascertain accuracy of results. The zone of inhibition was observed and recorded in millimetre.

3. Results and discussion

Different concentrations of silver nitrate solutions yielded nano silver with AK, SK, PGK, PAK, SF, ARL, AC, APC and KFL extracts within 20–30 min. During sonication, the production of increased reactive sites with increase in temperature is followed by rapid cooling. This avoids evaporation of solvents that is noticed in higher temperature conditions. Quick synthesis (5 min) of AgNPs was obtained using MP and RM extracts whereas, OB and TH extracts takes 15 min for the formation of AgNPs. PG, WH and CR produce AgNPs in 35–45 min. This discloses the effect of ultrasonic waves on the reaction mixture. The active compounds such as saponins,

steroids, terpenoids *etc.* are extracted three times faster using ultrasonication than the traditional one. This may be the reason for the rapid reduction of silver ions by the metabolites present in the plant extracts.

3.1. UV–visible spectral analysis of silver nanoparticles

The UV–Visible spectra of the synthesized AgNPs using a constant volume (1 ml) of eight plant extracts (AK, SK, PGK, PAK, RM and MP)

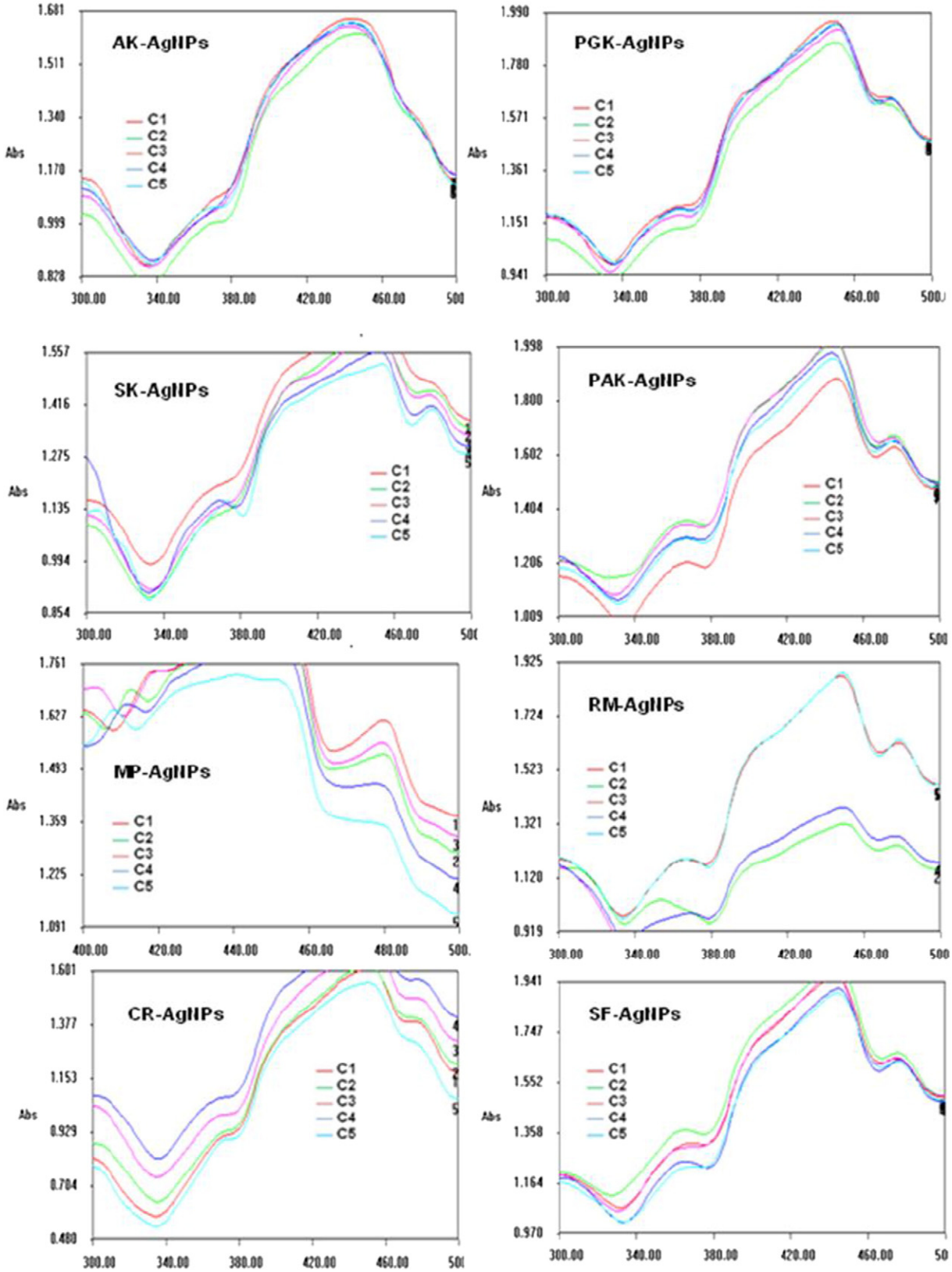

Fig. 1. UV–Visible spectra of AgNPs synthesized using AK, PGK, SK, PAK, MP, RM, CR and SF extracts.

with different concentrations of $AgNO_3$ (6, 7, 8, 9 and 10 ml) under sonication are given in Fig. 1. The SPR bands at 440, 448, 445, 440, 450 and 425 nm correspond to nanosilver synthesized using aqueous extracts of AK, SK, PGK, PAK, RM and MP respectively (Fig. 1). The broad SPR band at 420–440 nm confirms the uniform distribution of AgNPs. The UV–Visible spectra of the APC, OB, CR, SF, AC and ARL showed broad band

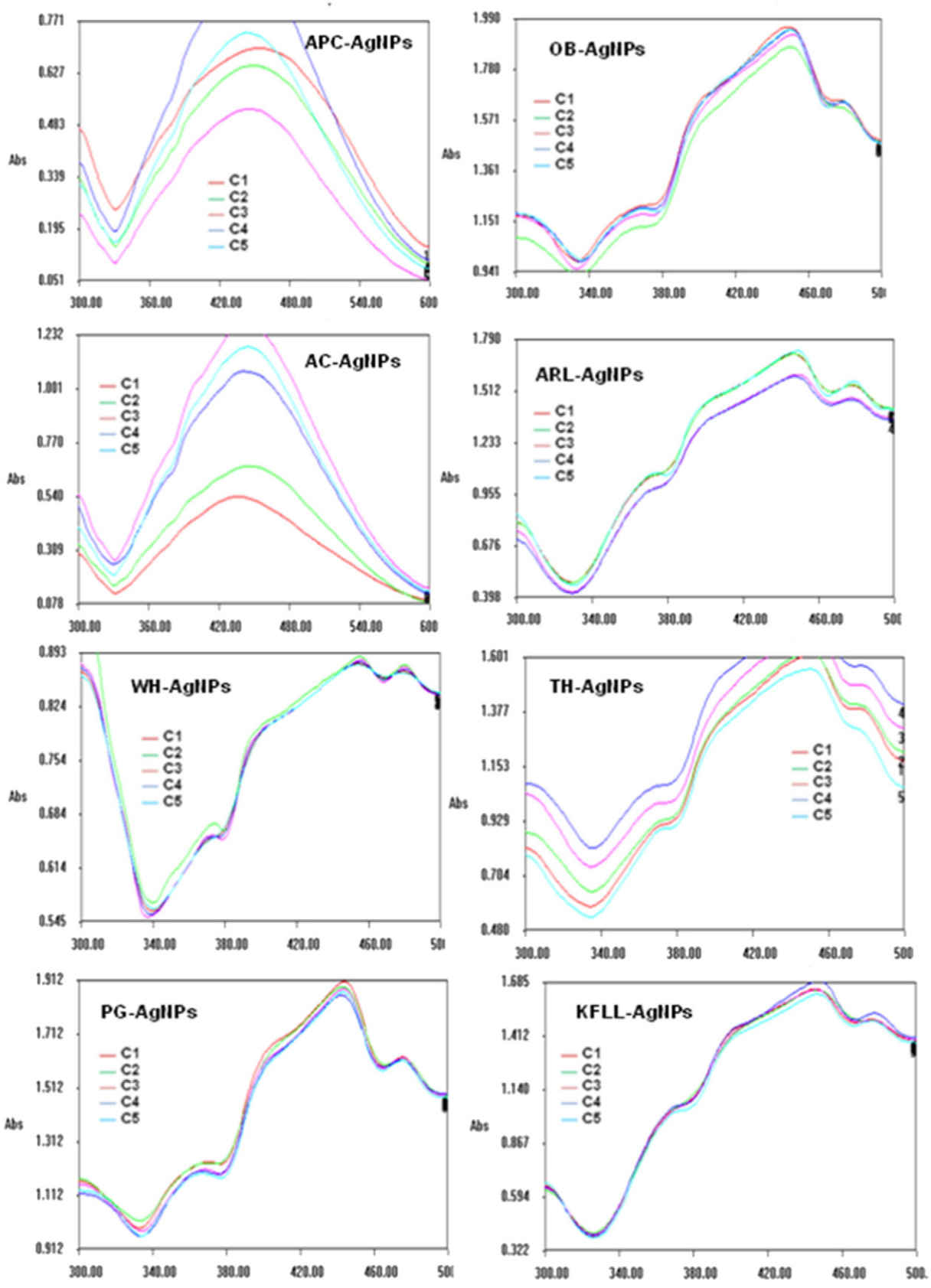

Fig. 2. UV–Visible spectra of AgNPs synthesized using APC, OB, AC, ARL, WH, TH, PG and KFL extracts.

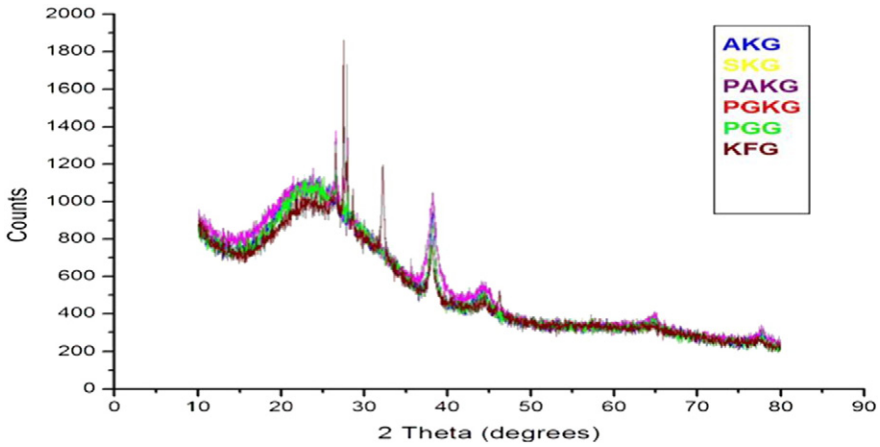

Fig. 3. XRD patterns of synthesized AgNPs using AK, SK, PGK, PAK, PG and KFL extracts.

at 420–460 nm revealing the formation of polydispersed AgNPs (Figs. 1 and 2).

The extinction maxima were observed at 360 and 440 nm and shoulders on the plasmon bands at 475 nm for SF, RM, PGK, ARL, KFL and PG-mediated AgNPs (Figs. 1 and 2). These bands explains the existence of two size fractions of AgNPs. The maximum absorption wavelength increases with the increasing of larger size AgNPs percentage volume. Such a red-shift is characteristic for an increased NPs size. The position of the absorption maximum of polydisperse colloid does not give information about the size of nanoparticles, because it is not possible to observe peaks separation form specific populations in these colloids. The plasmon resonance will be red-shifted to a longer wavelength for a multi-nanoparticle aggregate than the resonance of an individual nanoparticles [27]. Thus the aggregation is observable as an intensity increase in the near infrared region of the spectrum.

It is noted that the SPR band occurs at 420–460 nm and steadily increases in intensity as a function of concentration without any shift in the peak wavelength for the remaining plant-mediated AgNPs (Figs.1 and 2). The narrow band was clearly seen in the AgNPs synthesized using AK, PGK, PG, OB and SF extracts indicating the uniform distribution with a lesser diameter of particles (Figs. 1 and 2).

WH and KFL-mediated AgNPs shows a broad band at 420–460 nm for the solution containing 5 ml of plant extracts and varied concentrations of $AgNO_3$. A sharp band at 430 nm was observed for the PG-AgNPs and TH-AgNPs synthesized using the aforesaid concentration of these extracts. The SPR bands vary with different plant-mediating AgNPs although the colour obtained was reddish-brown. This implies the role and nature of reducing and capping agents present in the plant extracts.

The increase in the concentration of silver nitrate widens the UV band and the intensity is strengthened apparently for most of the synthesized AgNPs. Similar results were observed for Aloe leaf-assisted synthesis of AgNPs [28]. The results were similar to that of the *Cinnamomum camphora* leaves and *Cinnamon zeylanicum* bark extract mediated AgNPs [29,30]. Silver NPs have unique optical properties because they support surface plasmons. At specific wavelengths of light the surface plasmons are driven into resonance and the AgNPs have a distinct colour that is a function of their size, shape and environment [31,32].

As the quantity of the silver ions increase in synthesis, the formation of silver nanoparticles increased, thereby resulting in increased intensity of SPR bands. This is due to the higher content of the metal ions interaction with the phytochemicals that aids metal reductive process. All the synthesized AgNPs, observed for a 3 month period of time showed no discolouration or agglomeration suggesting its excellent stability. This stability evidences the presence of phytochemicals capped onto the synthesized nanosilver.

3.2. XRD analysis of silver nanoparticles

Fig. 3 portrays the XRD patterns of the synthesized AgNPs using the aqueous extracts of AK, SK, PGK, PAK, PG and KFL. The diffraction peaks at $2\theta = 38°$, 44°, 64° and 77° noted for the biosynthesized

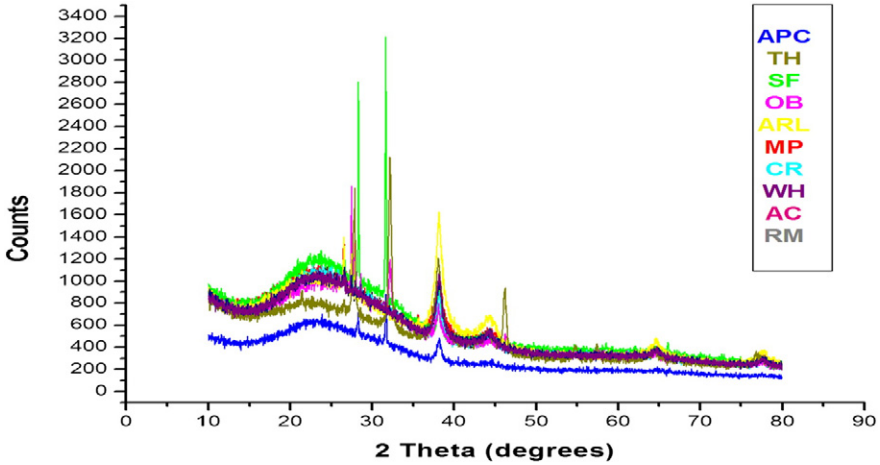

Fig. 4. XRD patterns of synthesized AgNPs using APC, TH, SF, OB, ARL, MP, CR, WH, AC and RM extracts.

AgNPs, correspond to the (111), (200), (220) and (311) planes of face-centered cubic lattice of nanosilver respectively. The XRD patterns show one intense peak of Bragg's reflection with 2θ values of 32° which may be due to the presence of a mixed phase of Ag/Ag_2O for SF, APC, TH and OB-mediated AgNPs (Fig. 4). A similar result was obtained for the morphological evolution of Ag_2O from cubes to octapods by a simple precipitation method [33].

Four intense and sharp peaks at 2θ = 38°, 44°, 64° and 77° were obtained corresponding to the 111, 200, 220, 311 and planes of Bragg's reflection of silver respectively, for AgNPs synthesized using SF, TH, OB, ARL, MP, CR, ARL, AC, WH and RM. The 2θ = 77° peak was absent in APC-mediated AgNPs indicating the formation of spherical-shaped AuNPs (Fig. 4). The additional peaks may be that of the capping agents or secondary metabolites present in the

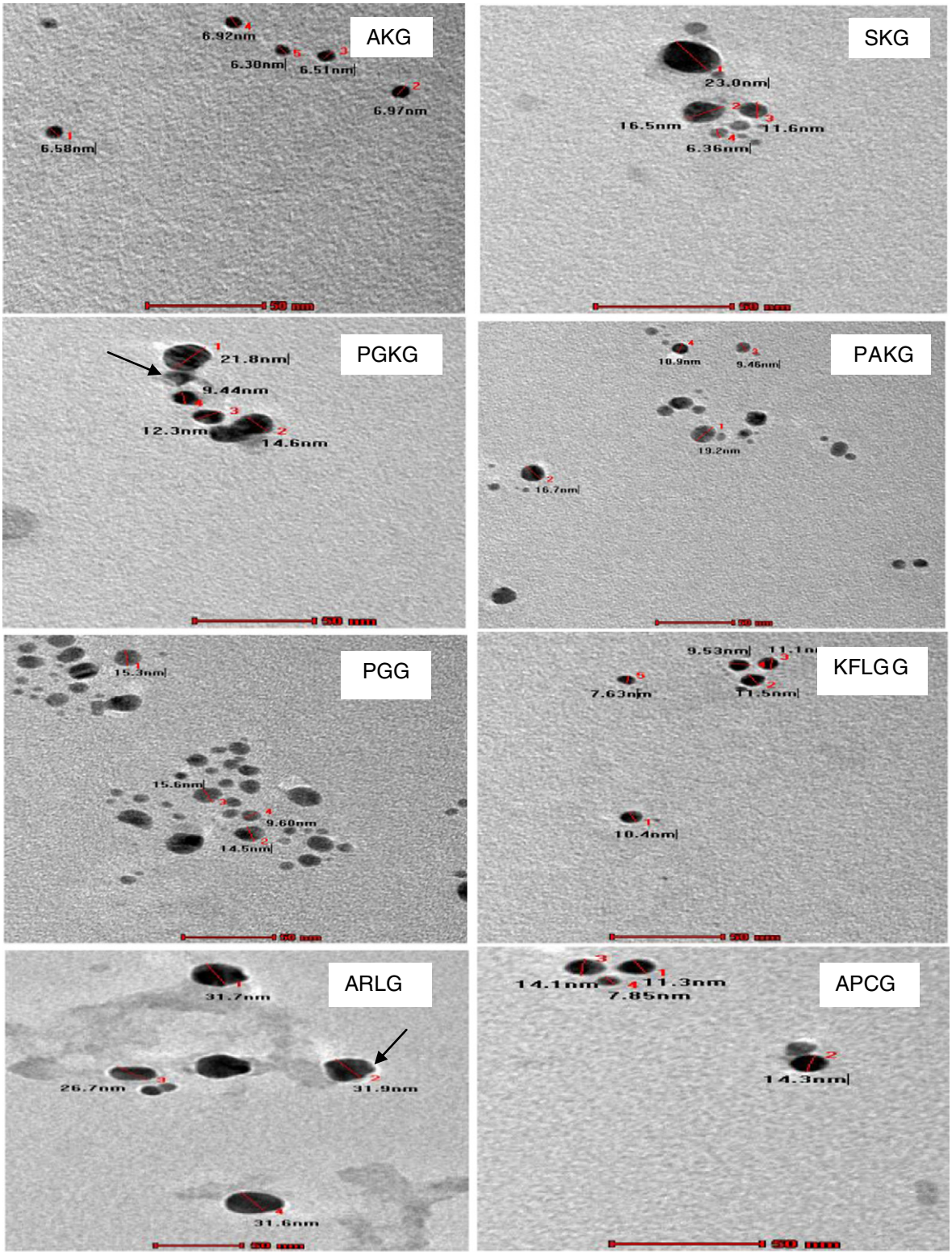

Fig. 5. TEM micrographs of AgNPs synthesized using AK, SK, PGK, PAK, PG, KFL, ARL and APC extracts.

AgNPs solutions. The XRD data confirm the crystalline nature of the synthesized AgNPs formed using these plant extracts similar to that of Joint Committee on Powder Diffraction Standards (JCPDS) No. 04–0783.

The XRD spectrum of AgNPs synthesized by wet chemical solution method revealed peaks at 2θ values 38.1°, 44.09°, 64.36°, 77.29°, 81.31°, 97.92°, 110.81° and 114.61° corresponding to (111), (200), (220), (311), (222), (400), (331) and (420) planes of silver, respectively revealing its crystalline structure [34]. Similar results were obtained for the AgNPs produced using extracts of *Strychnos potatorum* [35], *Carica papaya* [36] and *Argemone mexicana* [37]. The XRD patterns (Figs. 3 and 4) of the AgNPs

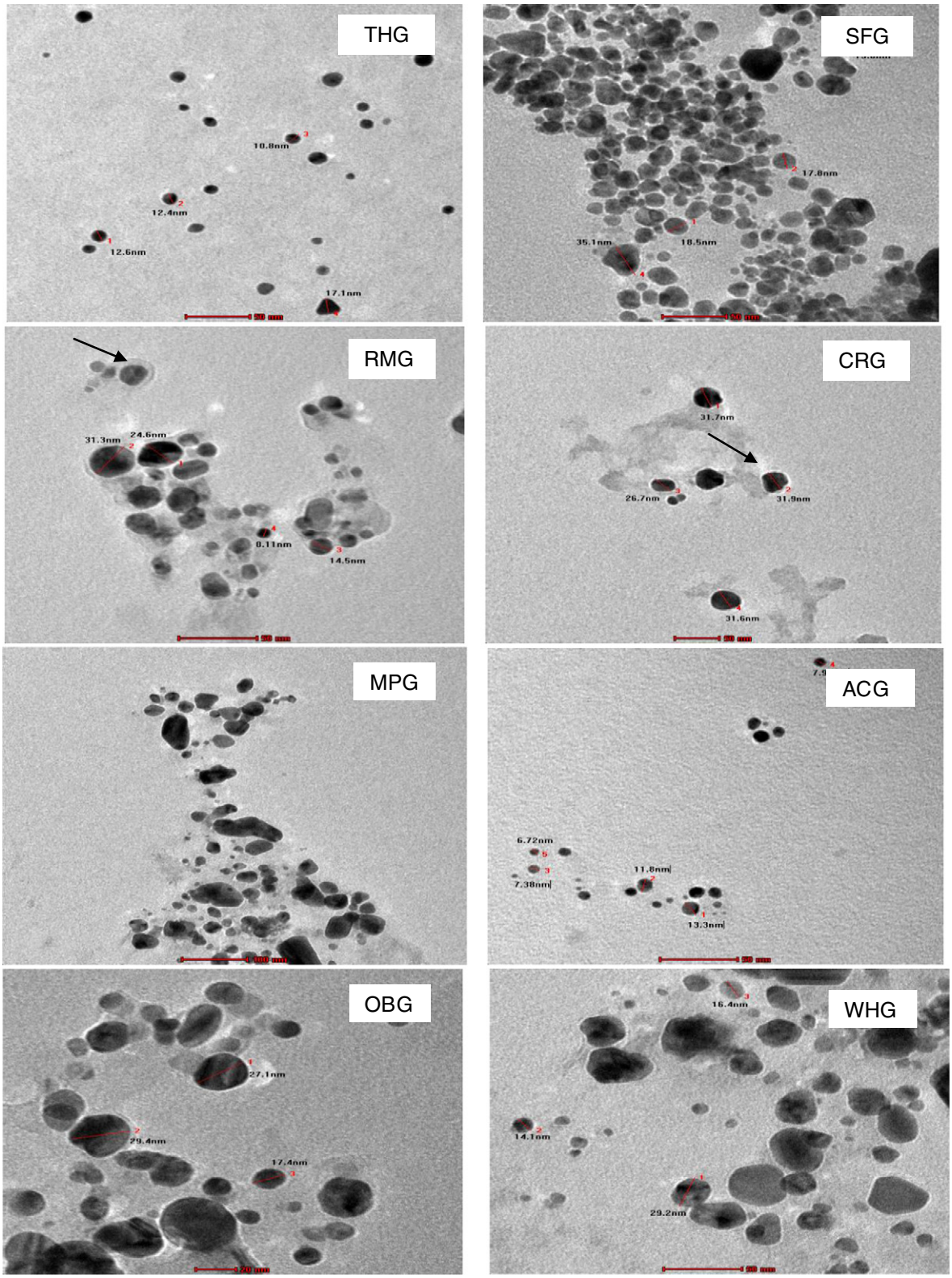

Fig. 6. TEM micrographs of AgNPs synthesized using TH, SF, RM, CR MP, AC, OB and WH extracts.

obtained in this research work too clearly illustrates the face-centered cubic lattice and crystalline nature of silver nanoparticles.

3.3. TEM analysis

Transmission Electron Microscopy (TEM) has the advantage over SEM that cellular structures of the specimen can be viewed at very high magnifications [38]. TEM images of the synthesized AgNPs were recorded to ascertain its shape and size. These images further confirmed the formation of spherical AgNPs of uniform distribution without agglomeration (Fig. 5). The particle sizes of the synthesized AgNPs were found to be 5–25 nm for AKG, SKG, PAKG, PGKG, PGG and KFLG (Figs. 5 and 6). RMG, CRG, SFG, ACG and ARLG exhibit particle sizes of <50 nm as confirmed from TEM images (Figs. 5 and 6).

The increase in the diameter of particle size due to the capping nature of the phytoconstituents is evidently seen in the TEM micrographs. Hence the biomolecule-capped AgNPs possesses good stability. The TEM images of APCG and THG showed spherical-shaped nanoparticles of size 10–20 nm. Irregular shapes of AgNPs of below 50 nm size were found for the WHG, MPG and OBG (Fig. 6). All the biosynthesized AgNPs exhibits spherical and quasi spherical-shaped of size below 50 nm except WHG, MPG and OBG which are irregular in shape (Fig. 6). ACG, ARLG, RMG and PGKG embedded with protein molecules as capping agents contributing to the stability of synthesized AgNPs, are indicated by black arrow in Figs. 5 & 6. The TEM results correlated well with the SPR band and XRD analysis. Nanoparticles of size <100 nm are anticipated to have a high surface area and good pharmacological and biological activity like antimicrobial activity. The TEM images reveal the prospective applications of the biosynthesized AgNPs.

3.4. Antibacterial activity of the biosynthesized AgNPs against E. coli, S. paratyphi, S. aureus and B. subtilis

The antibacterial activity of the sixteen biosynthesized AgNPs against *E. coli, S. paratyphi, S. aureus* and *B. subtilis* revealed excellent antibacterial activity against tested bacterial strains at the volume of 20 μl / 600 μg AgNPs/well (Table 2 and Fig. 7).

The *anti- E. coli* activity of PGKG, SFG and RMG (24 mm) were almost double compared to that of standard Gentamicin (12 mm). The activity of all other AgNPs was greater than or equal to that of standard. PGKG revealed highest zone of inhibition (29 mm) against *E. coli.* The anti-*S.aureus* activity was found to be highest (24 mm) with MPG while PAKG, WHG and SFG showed 23 mm compared to 16 mm zone of inhibition of standard. All other AgNPs showed greater activity against *S. aureus* compared to standard except OBG. The anti-*S.paratyphi* activity of PGKG, PAKG and SFG was nearly doubled compared to that of standard (12 mm).

The other AgNPs exhibit highest zone of inhibition except OBG against *S. paratyphi* compared to that of standard. WHG, SFG, ARLG and OBG showed highest zone of inhibition (21 mm) to that of standard (14 mm) against *B. subtilis*. The anti- *B. subtilis* activity of all other AgNPs was greater than or equal to that of standard. SFG exhibit highest zone of inhibition against *E. coli, S. paratyphi, S. aureus* and *B. subtilis* compared to all other AgNPs and standard.

The presence of metabolites like flavonoids, tannins, saponins, carbohydrates, proteins, *etc.* in the embedded-SFG may be responsible for the greater antibacterial activity than other AgNPs. PGKG showed good zone of inhibition against *E. coli* (29 mm) and *S. paratyphi* (25 mm). PAKG exhibits greater activity compared to all other AgNPs and standard against *S. paratyphi* and *S. aureus.*

The particle sizes of the synthesized AgNPs were found to be 5–25 nm for AKG, SKG, PAKG, PGKG, PGG and KFLG (Figs. 5 and 6). RMG, CRG, SFG, ACG and ARLG exhibit particle sizes of <50 nm as confirmed by TEM images (Figs. 5 and 6). All the biosynthesized AgNPs exhibits spherical and quasi spherical shape of size below 50 nm except WHG, MPG and OBG which are irregular in shape. Hence, the aforesaid biosynthesized AgNPs are comprised of polydispersed particles as shown in earlier results. However, AKG, SKG, PAKG, PGKG, PGG and KFLG are of smaller-size compared to WHG, MPG and OBG which are trapped at the edge of the agar well. Only small-sized particles might have diffused through agar exhibiting good antimicrobial activity against the tested bacteria. The method of the synthesis for all 16 AgNPs is the same and the capped biomolecules might be more or less similar with slight modifications, because of the differences in plant sources. The nature of similar capping agents in AKG, SKG, MPG, WHG and ARLG probably gives similar results in its antimicrobial activity study.

Iresine herbstii-mediated AgNPs give zone of inhibition 15.7 and 14.8 mm against *E. coli* and *S. aureus* respectively at a concentration 250 μg/ ml [39]. **Prasad and Swamy** (**2013**) have reported growth inhibition (11 and 18 mm) against *E. coli* and *S. aureus* respectively, for the AgNPs synthesized using *Syzgium cumini* [40]. The diameter of the inhibition zone denotes the relative susceptibility of the test microorganisms to a particular test substance [41].

Zone of Inhibition (mm)	Type of antimicrobe
> 13	Highly sensitive or susceptible
8–13	Moderately sensitive or intermediate
< 8	Resistant

The results of the present antibacterial activity reveal all plant-mediated AgNPs to show zone of inhibition > 13 indicating highly susceptible activity of AgNPs against the tested bacteria.

In the present study, the biosynthesized AgNPs showed better antibacterial activity against pathogenic bacteria compared to zone of inhibition values reported in literature. Therefore, the biosynthesized AgNPs (AKG, SKG, PAKG, PGKG, ARLG, THG, SFG, RMG, MPG, CRG, PGG, KFLG, ACG, APCG and WHG) are highly active against *E. coli, S. paratyphi, S. aureus* and *B. subtilis*. Only OBG was moderately sensitive against *E. coli, S. paratyphi* and *S. aureus*, but resistant towards *B. subtilis*.

3.5. Mechanism of inhibition of bacterial threats by AgNPs

The mechanism of the inhibitory effects of Ag ions on microorganisms is partially known. The free radicals generated by AgNPs induce damage to the bacterial cell membrane. Extracellular and intracellular system can also be damaged by the formation of reactive oxygen species by the interaction of AgNPs with water [42]. The antimicrobial effect of the AgNPs on gram-negative bacteria depends on the concentration of the AgNPs. It has the ability to attach to the bacterial wall, form pits on the wall and penetrate causing structural changes and finally death

Table 2
Results of antibacterial activity of biosynthesized silver nanoparticles.

S. No	Plant-mediated AgNPs	Zone of inhibition (Value = Mean ± SD) (mm)			
		E.coli	*S. aureus*	*S. paratyphi*	*B. subtilis*
1.	**STD (Gentamicin)**	**12 ± 1.0**	**16 ± 0.6**	**12 ± 0.5**	**14 ± 1.2**
2.	AKG	21 ± 0.5	18 ± 0.6	21 ± 0.5	18 ± 0.6
3.	SKG	21 ± 0.6	19 ± 1.0	23 ± 0.5	15 ± 0.6
4.	PAKG	22 ± 1.0	23 ± 0.5	**25** ± 1.0	20 ± 1.2
5.	PGKG	**29 ± 1.0**	22 ± 0.5	**25** ± 0.6	20 ± 0.5
6.	PGG	20 ± 0.6	16 ± 0.5	20 ± 0.5	17 ± 1.2
7.	KFLG	18 ± 0.5	19 ± 1.2	22 ± 0.5	14 ± 0.5
8.	APCG	16 ± 1.0	17 ± 1.2	19 ± 0.5	18 ± 0.6
9.	MPG	22 ± 0.5	**24** ± 0.5	23 ± 0.5	19 ± 1.2
10.	WHG	22 ± 1.0	23 ± 0.5	22 ± 0.5	**22** ± 0
11.	SFG	24 ± 0.6	23 ± 0.5	24 ± 0.6	21 ± 0.6
12.	RMG	26 ± 1.2	21 ± 0.5	21 ± 0.6	20 ± 0.6
13.	ARLG	22 ± 0.5	22 ± 0.6	23 ± 0.6	21 ± 0.5
14.	OBG	12 ± 1.2	9 ± 1.2	10 ± 1.7	17 ± 0.6
15.	CRG	20 ± 0.5	22 ± 0.6	20 ± 0.6	21 ± 0.5
16.	THG	20 ± 0.5	21 ± 0.6	23 ± 0.5	20 ± 0.5
17.	ACG	21 ± 0.6	20 ± 0.5	19 ± 0.5	18 ± 1.2

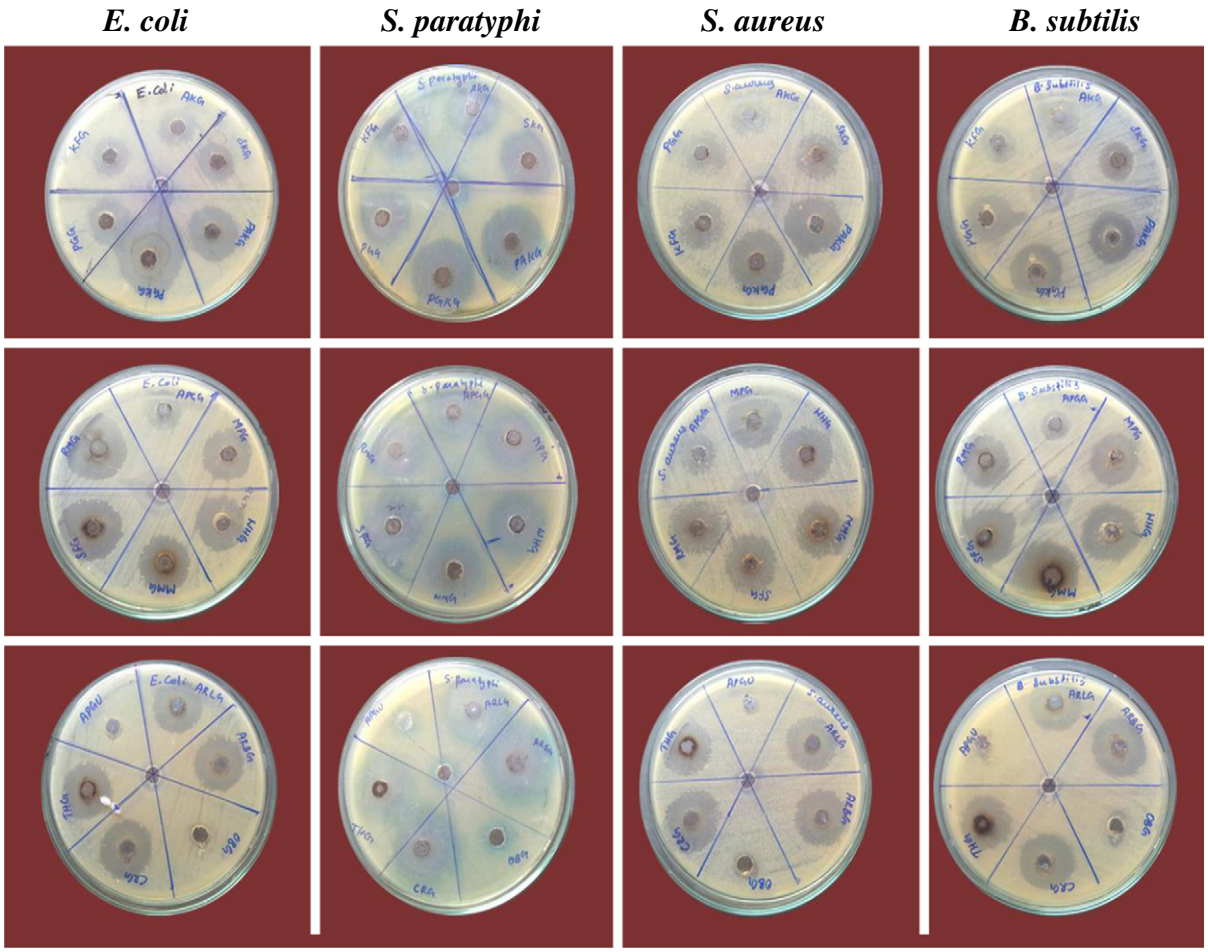

Fig. 7. Photograph of antibacterial activity of biosynthesized silver nanoparticles against *E. coli*, *S. paratyphi*, *S. aureus* and *B. subtilis*.

of cells [43]. The positive charge on the silver ion attracting the negatively charged cell membrane of microorganisms through the electrostatic interaction is also suggested as a reason for antimicrobial activity [44,45]. The turbulence of membrane permeability would be an important factor to inhibit the bacterial growth [46]. As the AgNPs enters into the bacterial cell, it preferably attacks the respiratory chain, prevent cell division and cell death [47].

The shape of the bacteria chosen for the study is different, hence the antibacterial activity also achieved by their respective morphological changes in the cell wall of the specific bacteria will also differ. The two modes of interaction of AgNPs on bacterial cell are through: i) formation of free radicals and ii) reactive oxygen species [48].

Thus the action model of AgNPs may be explained as AgNPs initially make a break through the permeability of the outer membrane which results in the leakage of cellular materials. Finally, AgNPs inhibits the respiration and growth of cells by entering the inner membrane and inactivating the respiratory chain dehydrogenases, simultaneously AgNPs could affect some proteins and phosphate lipids and induce collapse of membrane, resulting in cell decomposition and death eventually [49]. These results suggest that the toxicity of the AgNPs is the result of action inside and not on the bacteria. The extent of these effects is positively related to the concentration of AgNPs. The biosynthesized AgNPs may thus inhibit the bacterial growth probably by these mechanism.

4. Conclusion

All 16 plant extracts yielded AgNPs rapidly within few minutes under sonication method. The UV–Visible absorption spectral results of biosynthesized AgNPs showed SPR band at 420–470 nm indicating the formation of uniform size nanoparticles. XRD patterns of AgNPs confirmed the formation of cubic structure nanoparticles. TEM analysis of AK, SK, PAK, PGK, PG, APC, TH and KFL-mediated AgNPs showed spherical-shaped of size 5–25 nm whereas <50 nm was observed for RM, CR, SF, AC and ARL-AgNPs. Irregular shapes or quasi-spherical shaped AgNPs below 50 nm size were noted for the AgNPs synthesized using WH, MP and OB extracts. Significant antimicrobial activity was obtained for the biosynthesized AgNPs against selected bacterial threats. PGK-AgNPs are highly active against *E. coli* (29 mm), *S. paratyphi* (25 mm), *S. aureus* (22 mm) and *B. subtilis* (20 mm) compared to that of standard Gentamicin. OBG was moderately sensitive against *E. coli, S. paratyphi* and *S. aureus*, but resistant towards *B. subtilis*.

Conflict of interests

The authors declare that there is no conflict of interests regarding the publication of this paper.

Acknowledgement

The authors sincerely thank the Avinashilingam Institute for Home Science and Higher Education for Women, Coimbatore, for providing research facilities, Department of Physics, Avinashilingam University for Women, for recording XRD, KMCH College of Pharmacy for their assistance in the antibacterial study and Department of Nano Science and Technology, Tamil Nadu Agricultural University, for recording TEM.

References

[1] K.S. Mukunthan, E.K. Elumalai, T.N. Patel, V. Ramachandra Murty, *Catharanthus roseus*: a natural source for the synthesis of silver nanoparticles, Asian Pac. J. Trop. Biomed. 1 (2011) 270–274.

[2] P.K. Jain, K.S. Lee, I.H. El-Sayed, M.A. El-Sayed, Calculated absorption and scattering properties of gold nanoparticles of different size, shape, and composition: applications in biological imaging and biomedicine, J. Phys. Chem. B 110 (2006) 7238–7248.

[3] J. Liu, Y. Lu, Accelerated color change of gold nanoparticles assembled by DNAzymes for simple and fast colorimetric Pb2+ detection, J. Am. Chem. Soc. 126 (2004) 12298–12305.

[4] M.V. Yigit, Z. Medarova, *In vivo* and *ex vivo* applications of gold nanoparticles for biomedical SERS imaging, Am. J. Nucl. Med. Mol. Imaging 2 (2012) 232–241.

[5] M.J. Firdhouse, P. Lalitha, Fabrication of antimicrobial perspiration pads and cotton cloth using *Amaranthus dubius* mediated silver nanoparticles, J. Chem. (2013), 741743, http://dx.doi.org/10.1155/2013/741743 5 pages.

[6] Y. Yang, P. Burkhard, Encapsulation of gold nanoparticles into self-assembling protein nanoparticles, J. Nanobiotechnol. 10 (2012) 42.

[7] M.J. Firdhouse, P. Lalitha, Biosynthesis of silver nanoparticles and its applications, J. Nanotechnol. (2015), 829526, http://dx.doi.org/10.1155/2015/829526 18 pages.

[8] M.K. Teli, S. Mutalik, G.K. Rajanikant, Nanotechnology and nanomedicine: going small means aiming big, Curr. Pharm. Des. 16 (2010) 1882–1892.

[9] M.J. Firdhouse, P. Lalitha, Biocidal potential of biosynthesized silver nanoparticles against fungal threats, J. Nanostruct. Chem. 5 (2014) 25–33, http://dx.doi.org/10.1007/s40204-015-0042-2.

[11] M.J. Firdhouse, P. Lalitha, Biosynthesis of silver nanoparticles using the extract of *Alternanthera sessilis*—antiproliferative effect against prostate cancer cells, Cancer Nano. 4 (2013) 137–143, http://dx.doi.org/10.1007/s12645-013-0045-4.

[12] A. Ahmad, S. Senapati, M.I. Khan, R. Kumar, M. Sastry, Extracellular biosynthesis of monodisperse gold nanoparticles by a novel extremophilic actinomycete *Thermomonospora* sp, Langmuir 19 (2003) 3550–3553.

[13] M.C. Daniel, D. Astruc, Gold nanoparticles: assembly, supramolecular chemistry, quantum-size-related properties, and applications toward biology, catalysis, and nanotechnology, Chem. Rev. 104 (2004) 293–346.

[14] T. Joseph, R. Moore, Drug Delivery Using Nanotechnology Technologies: Markets & Competitive Environment, Tech. Rep, Institute of Nanotechnology, 2008.

[15] H. Kato, In vitro assays: tracking nanoparticles inside cells, Nat. Nanotechnol. 6 (2011) 139–140.

[16] D.L. Mager, Bacteria and cancer: cause, coincidence or cure? A review, J. Transl. Med. 4 (2006) 1–18.

[17] J. Cummins, M. Tangney, Bacteria and tumours: causative agents or opportunistic inhabitants? Infect. Agents Cancer 8 (2013) 1–8.

[18] C. Montalban, A. Santon, D. Boixeda, C. Bellas, Regression of gastric high grade mucosa associated lymphoid tissue (MALT) lymphoma after *Helicobacter pylori* eradication, Gut 49 (2001) 584–587.

[19] J. Biarc, I.S. Nguyen, A. Pini, F. Gosse, S. Richert, D. Thierse, D.A. Van, E. Leize-Wagner, F. Raul, J.P. Klein, M. Scholler-Guinard, Carcinogenic properties of proteins with pro-inflammatory activity from *Streptococcus infantarius* (formerly *S. bovis*), Carcinogenesis 25 (2004) 1477–1484.

[20] L. A.J., E. White, L.A. Jackson, M.D. Thornquist, C.A. Gaydos, G.E. Goodman, T.L. Vaughan, *Chlamydia pneumoniae* infection and risk of lung cancer, Cancer Epidemiol. Biomark. Prev. 13 (2004) 1624–1630.

[21] H.M. Martin, B.J. Campbell, C.A. Hart, C. Mpofu, M. Nayar, R. Singh, H. Englyst, H.F. Williams, J.M. Rhodes, Enhanced *Escherichia coli* adherence and invasion in Crohn's disease and colon cancer, Gastroenterol. 127 (2004) 80–93.

[22] C.P. Caygill, M.J. Hill, M. Braddick, J.C. Sharp, Cancer mortality in chronic typhoid and paratyphoid carriers, Lancet 343 (1994) 83–84.

[23] U. Dutta, P.K. Garg, R. Kumar, R.K. Tandon, Typhoid carriers among patients with gallstones are at increased risk for carcinoma of the gallbladder, Am. J. Gastroenterol. 95 (2000) 784–787.

[24] R. DeJong, F. Altare, I.A. Haagen, D.G. Elferink, T. Boer, P.J. Vriesman, P.J. Kabel, J.M. Draaisma, J.T. Van Dissel, F.P. Kroon, J.L. Casanova, T.H. Ottenhoff, Severe mycobacterial and *Salmonella* infections in interleukin-12 receptor-deficient patients, Science 280 (1998) 1435–1438.

[25] T.J. Montville, K.R. Matthews, Food Microbiology: An Introduction, second ed. ASM Press, Washington D.C., 2008

[26] FDA, Bad Bug Book: Foodborne Pathogenic Microorganisms and Natural Toxins Handbook, second ed. US Food and Drug Administration, Silver Spring, 2012 87–92.

[27] E. Tomaszewska, K. Soliwoda, K. Kadziola, B. Tkacz-Szczesna, G. Celichowski, M. Cichomski, W. Szmaja, J. Grobelny, Detection limits of DLS and UV–Vis spectroscopy in characterization of polydisperse nanoparticles colloids, J. Nanomater. (2013), 313081 10 pages.

[28] Y. Zhang, X. Cheng, Y. Zhang, X. Xue, Y. Fu, Biosynthesis of silver nanoparticles at room temperature using aqueous aloe leaf extract and antibacterial properties, Colloids Surf. A Physicochem. Eng. Asp. 423 (2013) 63–68.

[29] J.L. Huang, Q.B. Li, D.H. Sun, Y.H. Li, Y.B. Su, X. Yang, H.X. Wang, Y.P. Wang, W.Y. Shao, N. He, J.Q. Hong, C.X. Chen, Biosynthesis of silver and gold nanoparticles by novel sundried *Cinnamomum camphora* leaf, Nanotechnology 18 (2007) 105104.

[30] M. Sathishkumar, K. Sneha, S.W. Won, C.W. Cho, S. Kim, Y.S. Yun, *Cinnamon zeylanicum* bark extract and powder mediated green synthesis of nano-crystalline silver particles and its bactericidal activity, Colloids Surf. B: Biointerfaces 73 (2009) 332–338.

[31] C. Noguez, Surface plasmons on metal nanoparticles: the influence of shape and physical environment, J. Phys. Chem. C 111 (2007) 3806–3819.

[32] M.J. Firdhouse, P. Lalitha, S.K. Sripathi, An undemanding method of synthesis of gold nanoparticles using *Pisonia grandis* (R. Br.), Dig. J. Nanomater. Biostruct. 9 (2014) 385–393.

[33] M.J. Kim, S. Kim, H. Park, Y.D. Huh, Morphological evolution of Ag_2O microstructures from cubes to octapods and their antibacterial activities, Bull. Kor. Chem. Soc. 32 (2011), http://dx.doi.org/10.5012/bkcs.2011.32.10.3793.

[34] M.A.M. Khan, S. Kumar, M. Ahamed, S.A. Alrokayan, M. Saleh AlSalhi, Structural and thermal studies of silver nanoparticles and electrical transport study of their thin films, Nanoscale Res. Lett. 434 (2011), http://dx.doi.org/10.1186/1556-276X-6-434.

[35] S. Kagithoju, V. Godishala, R. Nanna, Eco-Friendly and Green Synthesis of Silver Nanoparticles Using Leaf Extract of *Strychnos potatorum* Linn.F. And their Bactericidal Activities, 3 Biotech, 2014, http://dx.doi.org/10.1007/s13205-014-0272-3.

[36] D. Jain, H.K. Daima, S. Kachhwaha, S.L. Kotharia, Synthesis of plant-mediated silver nanoparticles using papaya fruit extract and evaluation of their antimicrobial activities, Dig. J. Nanomater. Biostruct. 4 (2009) 723–727.

[37] A. Singh, D. Jain, M.K. Upadhyay, N. Khandelwal, H.N. Verma, Green synthesis of silver nanoparticles using *Argemone mexicana* leaf extract and evaluation of their antimicrobial activities, Dig. J. Nanomater Biostruct. 5 (2010) 483–489.

[38] C.T.K.H. Stadtländer, H. Kirchhoff, Microsc. Res. Tech. 28 (1994) 368.

[39] C. Dipankar, S. Murugan, The green synthesis, characterization and evaluation of the biological activities of silver nanoparticles synthesized from *Iresine herbstii* leaf aqueous extracts, Colloids Surf. B: Biointerfaces 98 (2012) 112-9a.

[40] R. Prasad, V.S. Swamy, Antibacterial activity of silver nanoparticles synthesized by bark extract of *Syzygium cumini*, J. Nanoparticles (2013), 431218 6 pages.

[41] P. Arulpriya, P. Lalitha, S. Hemalatha, Antimicrobial testing of the extracts of *Samanea saman* (Jacq.)Merr, Der Pharma Chem. 2 (2010) 73–83.

[42] J.S. Kim, E. Kuk, K.N. Yu, J.H. Kim, S.J. Park, H.J. Lee, S.H. Kim, Y.K. Park, Y.H. Park, Antimicrobial effects of silver nanoparticles, Nanomedicine Nanotechnol. 3 (2007) 95–101.

[43] I. Sondi, B. Salopek-Sondi, Silver nanoparticles as antimicrobial agent: a case study on *E. coli* as a model for gram-negative bacteria, J. Colloid Interface Sci. 275 (2004) 177–182.

[44] P. Dibrov, J. Dzoiba, K.K. Gosink, C.C. Häse, Chemiosmotic mechanism of antimicrobial activity of Ag(+) in *Vibrio cholera*, Antimicrob. Agents Chemother. 46 (2002) 2668–2770.

[45] T. Hamoud, A. Myc, B. Donovan, A. Shih, J.D. Reuter, R.J. Baker, A novel surfactant nanoemulsion with a unique non-irritant topical antimicrobial against bacteria, enveloped viruses and fungi, Microbiol. Res. 156 (2001) 1–7.

[46] W. Li, X. Xie, Q. Shi, H. Zeng, Y. Ou-Yang, Y. Chen, Antibacterial activity and mechanism of silver nanoparticles on *Escherichia coli*, Appl. Microbiol. Biotechnol. 85 (2010) 1115–1122.

[47] M. Rai, A. Yadav, A. Gade, Silver nanoparticles as a new generation of microbials, Biotech. Adv. 27 (2009) 76–83.

[48] A. Abbaszadegan, Y. Ghahramani, A. Gholami, B. Hemmateenejad, S. Dorostkar, M. Nabavizadeh, H. Sharghi, The effect of charge at the surface of silver nanoparticles on antimicrobial activity against gram-positive and gram-negative bacteria: a preliminary study, J. Nanomater. (2015), 720654 8 pages.

[49] W.R. Li, X.B. Xie, Q.S. Shi, H.Y. Zeng, Y.S. Ou-Yang, Y.B. Chen, Antibacterial activity and mechanism of silver nanoparticles on *Escherichia coli*, Appl. Microbiol. Biotechnol. 85 (2010) 1115–1122.